

RESEARCH

Open Access



Studies on the thermal sensitivity of lung cancer cells exposed to an alternating magnetic field and magnesium-doped maghemite nanoparticles

Malgorzata Sikorska^{1*}, Grzegorz Domanski², Magdalena Bamburowicz-Klimkowska¹, Artur Kasprzak³, Anna M. Nowicka⁴, Monika Ruzicka-Ayoush¹ and Ireneusz P. Grudzinski¹

*Correspondence:
malgorzata.sikorska@wum.edu.pl

¹ Department of Toxicology and Food Science, Faculty of Pharmacy, Medical University of Warsaw, Banacha Str. 1, 02-097 Warsaw, Poland

² Institute of Radioelectronics and Multimedia Technology, Faculty of Electronics and Information Technology, Warsaw University of Technology, Nowowiejska Str. 15/19, 00-665 Warsaw, Poland

³ Department of Organic Chemistry, Faculty of Chemistry, Warsaw University of Technology, Noakowskiego Str. 3, 00-664 Warsaw, Poland

⁴ Department of Inorganic and Analytical Chemistry, Faculty of Chemistry, University of Warsaw, Pasteura Str. 1, 02-093 Warsaw, Poland

Abstract

Background: Magnetic fluid hyperthermia (MFH) represents a promising therapeutic strategy in cancer utilizing the heating capabilities of magnetic nanoparticles when exposed to an alternating magnetic field (AMF). Because the efficacy and safety of MFH treatments depends on numerous intrinsic and extrinsic factors, therefore, the proper MFH setups should focus on thermal energy dosed into the cancer cells.

Methods: In this study, we performed MFH experiments using human lung cancer A549 cells (in vitro) and NUDE Balb/c mice bearing human lung (A549) cancer (in vivo). In these two experimental models, the heat was induced by magnesium-doped iron(III) oxide nanoparticles coated with mPEG-silane ($\text{Mg}_{0.1}\text{-}\gamma\text{-Fe}_2\text{O}_3(\text{mPEG-silane})_{0.5}$) when exposed to an AMF.

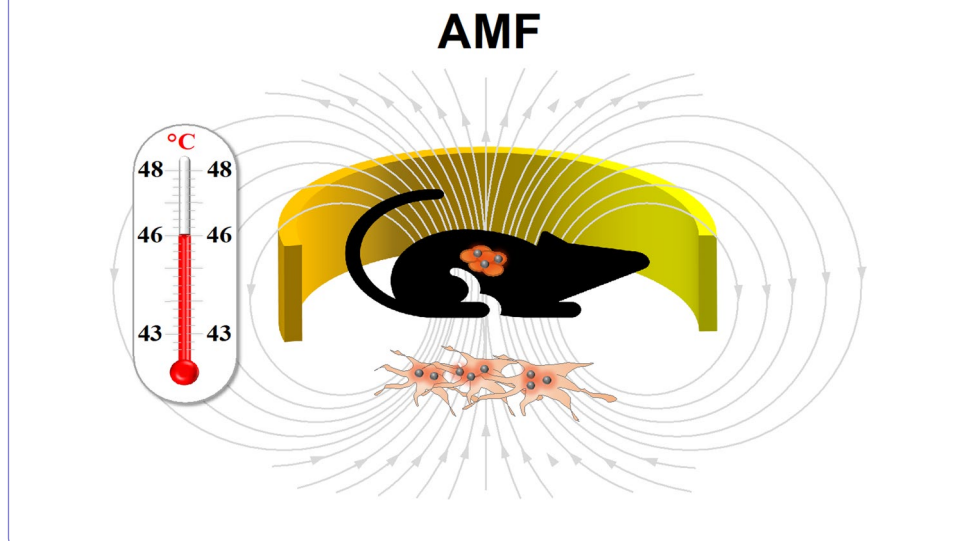
Results: We observed that the lung cancer cells treated with $\text{Mg}_{0.1}\text{-}\gamma\text{-Fe}_2\text{O}_3(\text{mPEG-silane})_{0.5}$ ($0.25\text{ mg}\cdot\text{mL}^{-1}$) and magnetized for 30 min at $14.4\text{ kA}\cdot\text{m}^{-1}$ yielded a satisfactory outcome in reducing the cell viability up to ca. 21% (in vitro). The activation energy calculated for this field strength was estimated for $349\text{ kJ}\cdot\text{mol}^{-1}$. Both volumetric measurements and tumor mass assessments confirmed by magnetic resonance imaging (MRI) showed a superior thermal effect in mice bearing human lung cancer injected intratumorally with $\text{Mg}_{0.1}\text{-}\gamma\text{-Fe}_2\text{O}_3(\text{mPEG-silane})_{0.5}$ nanoparticles ($3\text{ mg}\cdot\text{mL}^{-1}$) and subjected to an AMF ($18.3\text{ kA}\cdot\text{m}^{-1}$) for 30 min four times at weekly intervals. Research demonstrated that mice undergoing MFH exhibited a marked suppression of tumor growth ($V = 169 \pm 94\text{ mm}^3$; $p < 0.05$) in comparison to the control group of untreated mice. The CEM43 (cumulative number of equivalent minutes at $43\text{ }^\circ\text{C}$) value for these treatments were estimated for ca. 9.6 min with the specific absorption rate (SAR) level ranging from 100 to $150\text{ W}\cdot\text{g}^{-1}$.

Conclusions: The as-obtained results, both cytotoxic and those related to energy calculations and SAR, may contribute to the advancement of thermal therapies, concurrently indicating that the proposed magnetic fluid hyperthermia holds a great potential for further testing in the context of medical applications.



Keywords: Lung cancer, Thermal dose thresholds, Magnetic fluid hyperthermia, Iron oxide nanoparticles

Graphical Abstract



Introduction

Cancer is a leading global cause of mortality, with lung cancer alone accounting for approximately 350 deaths daily (Siegel et al. 2023). There are numerous cancer treatments such as chemotherapy, radiotherapy, immunotherapy or surgery, but all of them have some side effects, therefore, new therapeutic strategies are still developed (Fan et al. 2017). One of the methods employed in cancer treatments is hyperthermia, which is applied as a stand-alone treatment or adjuvant therapy (Altintas et al. 2021; Diederich and Hynynen 1999; Mantso et al. 2018; Shirvalilou et al. 2021). One of the types of hyperthermia frequently studied is magnetic fluid hyperthermia (MFH), which utilizes magnetic nanoparticles as a trigger for heat generation when subjected to an alternating magnetic field (AMF) (Habash et al. 2006; Jordan et al. 1999). The primary benefit of MFH among other hyperthermia treatments in generally lies in its ability to penetrate deep solid tissues due to magnetic nanoparticles when subjected to an AMF resulting in selectively eliminating cancer cells while preserving the normal cells with few side effects (Kozissnik et al. 2013; Liu et al. 2020). The efficacy and safety of MFH therapy depends significantly on numerous intrinsic and extrinsic factors, therefore, the proper magnetic hyperthermia setups should focus on the optimal thermal energy dosed into the target cells and tissues (Brollo et al. 2021; Catherine and Adam 2003; Kumar and Mohammad 2011; Obaidat et al. 2019).

The ultimate outcome of employing thermal therapies depends, among other factors, on the heterogeneity of multiple morphological and physiological aspects of the solid tumor and its microenvironment (Hirata and Sahai 2017; Jaeger et al. 2015; Marusyk and Polyak 2010). The variability of the molecular and cellular composition of lung cancer poses a significant challenge when considering therapeutic consequences (Zito Marino et al. 2019). Moreover, the diversity in molecular characteristics among

patients with the same histotype of lung cancer represents often leading to varying treatment responses (Jamal-Hanjani et al. 2015). In addition to MFH therapies, cancer cells also exhibit diverse reactions to heat exposures, which is a unique phenomenon in hyperthermia studies. As noted by Scutigliani et al., mounting evidence suggests that physiological responses to hyperthermia impact the tumor microenvironment (Scutigliani et al. 2021). Therefore, the introduction of the objective thermal dose concept seeks to establish a direct predictive correlation between the dosage quantity and the associated biological thermal damage outcomes resulting from heat exposure in cancer (Dewhirst et al. 2003a).

The proper transfer of thermal energy into the target cancer cells or tissues is still a real challenge in MFH (Chamani et al. 2023). Because the absorbed thermal energy is usually depleted non-homogeneously in a solid tumor, the intricacy of different biological factors such as cell types or even local vasculatures may affect such processes. It should be noted that cancer cells in the cell culture (in vitro) and solid tumors in the body (in vivo) represent different biological environments that may respond in specific ways when exposed to an AMF (Ruzycka-Ayoush et al. 2023). Therefore, heat penetration and heat transfers within cellular mass are considered as critical factors to be estimated for effective MFH therapies in preclinical studies before first-in-human trials. In recent years, there has been a growing interest in synthesizing of surface-functionalized and core-doped iron oxide nanoparticles with some unique properties such as efficient thermal effects (Lu and Hsiao 2023; Tran et al. 2015). Since iron nanoparticles distributed into cancer cells may generate heat when exposed to AMF, the major challenge of the present study is to estimate the thermal energy added to lung cancer cells that affects the overall cell survival required for effective anticancer treatment during the MFH therapy. Our recent studies evidenced that iron oxide nanoparticles both magnetite (Fe_3O_4) and maghemite ($\gamma\text{-Fe}_2\text{O}_3$) non-selectively affect the cancerous and non-cancerous lung cells leading to different cellular responses when subjected to an AMF. We also found that magnesium-doped maghemite nanoparticles ($\text{Mg}_{0.1}\text{-}\gamma\text{-Fe}_2\text{O}_3(\text{mPEG-silane})_{0.5}$) pronounced the thermal effects as compared to non-doped $\gamma\text{-Fe}_2\text{O}_3$ nanoparticles in lung cancer cells (Ruzycka-Ayoush et al. 2023). The significant enhanced heat induction was also observed by Jang et al. (Jang et al. 2018), who used $\text{Mg}_{0.13}\text{-}\gamma\text{-Fe}_2\text{O}_3$ nanoparticles for studies on malignant glioma cells (U87MG) in vitro and human liver adenocarcinoma (Hep3B) as xenografts in NUDE mice. Because the thermal sensitivity of lung cancer cells was not studied to date, as is available, for example, for brain tumors (Rodrigues et al. 2020), bladder cancer (Oliveira et al. 2013) or breast cancer (Wang et al. 2014), we focused here to study the activation energy and thermal dose thresholds elucidating the most promising heat penetration and heat mass transfer for effective damages of lung cancer cells and lung cancer tissues in a solid tumor exposed to $\text{Mg}_{0.1}\text{-}\gamma\text{-Fe}_2\text{O}_3(\text{mPEG-silane})_{0.5}$ nanoparticles and subjected to an AMF in both cellular (in vitro) and animal xenograft (in vivo) models. Understanding thermal sensitivity of lung cancer cells and the heating efficiency of nanoparticles subjected to an AMF may provide valuable insights into designing and optimizing the protocol for magnetic fluid hyperthermia, including such parameters as optimal temperature, exposure duration, and magnetic field strengths. It is our hope that setting out the thermal sensitivity of lung cancer cells

may prove to be useful for further studies, and that in the near future we might see first clinical trials of therapeutic magnetic hyperthermia addressing to this type of malignancy.

Experimental section/materials and methods

Iron(III) oxide nanoparticles doped with magnesium

Magnesium-doped iron(III) oxide nanoparticles coated with mPEG-silane via the formation of O–Si–C covalent bonds ($\text{Mg}_{0.1}\text{-}\gamma\text{-Fe}_2\text{O}_3(\text{mPEG-silane})_{0.5}$) were synthesized using the thermal decomposition method, as comprehensively described in our recent publication (Nowicka et al. 2023). The corresponding physicochemical and magnetic characterization was conducted using methods such as scanning and transmission electron microscopy, energy-dispersive X-ray spectroscopy, among others. The average size of a single as-synthesized nanoparticle was determined to be approximately 27 nm, with a magnetic saturation of 70 emu g^{-1} (Nowicka et al. 2023).

Magnetic fluid hyperthermia in cell studies

Human adenocarcinomic alveolar basal epithelial cell line, A549 (ATCC CCL-185) was obtained from the American Type Culture Collection (ATCC, Manassas, VA, USA). The A549 cells were grown as an adherent monolayer in F-12 K medium (Kaighn's modification of Ham's F-12 medium; Gibco, Paisley, supplemented with 10% fetal bovine serum (FBS; Gibco, Paisley, UK) and antibiotics (streptomycin, $50 \mu\text{g}\cdot\text{mL}^{-1}$; amphotericin B, $1.25 \mu\text{g}\cdot\text{mL}^{-1}$; gentamicin, $50 \mu\text{g}\cdot\text{mL}^{-1}$; penicillin, $50 \mu\text{g}\cdot\text{mL}^{-1}$) (Gibco, Paisley, UK). For the MFH cell studies, the cells were trypsinized (0.25% trypsin/EDTA solution; Gibco, Paisley, UK) and then plated in a 35-mm Petri dish. The cells were cultivated in a CO_2 incubator (Memmert, Schwabach, Germany) with a humidified atmosphere at 37°C , 5% CO_2 , and 90% humidity. The A549 cells plated in a 35-mm Petri dish (Falcon; Corning, Durham, NC, USA) at a density of 5×10^4 cells per dish in 2 mL volume of F-12 medium, were incubated for 24 h for adhesion. The adherent A549 cells were exposed to 0.2 mL of $\text{Mg}_{0.1}\text{-}\gamma\text{-Fe}_2\text{O}_3(\text{mPEG-silane})_{0.5}$ nanoparticles solution (providing a final concentration of $0.25 \text{ mg}\cdot\text{mL}^{-1}$), the dish was putted in support stand made by expanded polystyrene and further magnetized for 45 min with exposing to an alternating magnetic field. Non-magnetized cells treated with and without $\text{Mg}_{0.1}\text{-}\gamma\text{-Fe}_2\text{O}_3(\text{mPEG-silane})_{0.5}$ nanoparticles ($0.25 \text{ mg}\cdot\text{mL}^{-1}$) were served as controls. The rise of the sample temperature in the culture medium was measured by using a fiber-optic thermometer (Osensa™). The experimental setup for magnetization is shown in Table 1. Both magnetized and non-magnetized cells were incubated for 24 h and used for the cytotoxicity assay based on Alamar Blue (AB).

Alamar blue assay

The assessment of cell viability was conducted using the Alamar Blue assay. This assay generally monitors the reduction of resazurin under viable cellular conditions. Resazurin, which is the active compound in the Alamar Blue assay, specifically permeates viable cells and undergoes reduction to produce the intensely fluorescent resorufin (Rampersad 2012).

Table 1 Parameters of magnetization setup for magnetic fluid hyperthermia in lung cancer cells (in vitro) and NUDE Balb/c mice (in vivo) studies*

Magnetic induction value B [mT]	Magnetic field strength H_0 [$\text{kA}\cdot\text{m}^{-1}$]	$H \times f$ ($\leq 5 \cdot 10^9$ $\text{A}\cdot\text{ms}^{-1}$)
14	11.2	1.2×10^9
16	12.8	1.4×10^9
18	14.4	1.5×10^9
23	18.3	2.0×10^9

The study utilized a capacitor with a capacitance of 200 nF. The generated frequency f was 110.1 kHz. The last column is presented to compare the parameters used with the limit set by Hergt and Dutz, i.e., safety limits (Hergt et al. 2006)

*The system used for magnetic fluid hyperthermia consists of the central magnetization unit called magneTherm™ (nanoTherics Ltd.), CPX400SP 420W DC Power Supply, TG2000 20 MHz DDS Function Generator, SDS 1022 DL Digital Storage Oscilloscope and Induction Heating Coil with 17 turns of inner diameter 44 mm and cut around hollow cylinder inner side. To keep the coil temperature at the incubator temperature (37 °C), a water circulation inside the coil was provided, connecting to the water jacket using Grant LT ECOCOL 150 Electronic Thermostat System (Grant Instruments Ltd.)

After incubation, the control medium and the investigated magnetic nanoparticles were removed from dishes. The cells were rinsed twice with PBS, and 1 mL of Alamar Blue solution (10% [v/v] solution of Alamar Blue dye in fresh medium) was transferred to each dish. Following 3 h of incubation, the Alamar Blue fluorescence was quantified using an Epoch microplate reader (BioTek) at an excitation and emission wavelength of 560 and 590 nm, respectively. The viability of cells was expressed as fluorescence counts in the presence of the test compound, which was recalculated as a percentage of the control cells (non-magnetized and non-treated with magnetic nanoparticles). Both non-magnetized and magnetized cells treated with and without magnetic nanoparticles were documented on Olympus EP50 inverted microscopy (Olympus™).

Magnetic fluid hyperthermia in animal studies

The preclinical experiments were performed in compliance with the Institutional Animal Care and Use Committee and conducted according to the law for the welfare of animals and regulations for the care and use of laboratory animals. Six-old male NUDE Balb/c mice purchased from Charles River Laboratories (Germany) were housed in a group of five in individually ventilated cages (IVC) with free access to a standard diet (Altromin) and water ad libitum, and they were placed to 12 h light/dark cycle. The animals were acclimated to the animal facility for at least one week prior to the experimental procedure and were injected into the right flank with $4 \cdot 10^6$ A549 cells suspended in 100 μL of the culture medium. On two-week post-implantation, the naïve mice bearing ca. 3–4 mm tumors were injected intratumorally (0.2 mL) with $\text{Mg}_{0.1}\text{-}\gamma\text{-Fe}_2\text{O}_3(\text{mPEG-silane})_{0.5}$ nanoparticles ($3 \text{ mg}\cdot\text{mL}^{-1}$) and subjected to an alternating magnetic field for 30 min. The experimental setup for magnetization parameters is shown in Table 1. The animals were thermally imaged using an infrared (IR) camera before magnetization and at 5-, 10-, 15-, 20-, and 30-min during magnetization. Subsequently, they were imaged for an additional 15 min without magnetic fields (the cooling period). The magnetization of animals was performed four times at weekly intervals. Before each magnetization, the animals were injected intratumorally (0.2 mL) with nanoparticles ($3 \text{ mg}\cdot\text{mL}^{-1}$). Non-magnetized mice dosed with and without nanoparticles were served as controls. On 24 h after the last magnetization in the respective group, the magnetized and non-magnetized (control)

mice were subjected to magnetic resonance imaging (MRI) to visualize both the tumor and its vasculature.

Transmission electron microscopy

The investigation was conducted using a TALOS F200X equipped with a High-Angle Annular Dark-Field detector (manufactured by FEI, presently under Thermo Fisher Scientific). In the cellular studies, A549 cells were fixed with 2.5% glutaraldehyde cacodylic buffer and incubated for 1 h. Subsequently, they were washed in 0.1 M cacodylic buffer. The cells were then postfixed in 1% OsO₄ in double-distilled water (ddH₂O) for 1 h and underwent three washes in ddH₂O. Following post-fixation, the samples were dehydrated through a graded series of ethanol (30%—10 min, 50%—10 min, 70%—24 h, 80%—10 min, 90%—10 min, 96%—10 min, anhydrous ethanol—10 min, acetone—10 min) and infiltrated with epon resin in acetone (1:3—30 min, 1:1—30 min, 3:1—2 h). The specimens were infused twice for 24 h in pure epon resin and polymerized for 24 h at 60 °C. Subsequently, 60-nm sections were prepared using an RMC ultramicrotome MTX and examined without contrast under the transmission electron microscope LIBRA 120 TEM (Zeiss). The images were captured by the Slow Scan CCD (Proscan) using EsiVision Pro 3.2 software (Soft Imaging Systems GmbH). Measurements were conducted using the analySIS[®] 3.0 image-analytical software (Soft Imaging Systems GmbH).

Magnetic resonance imaging

Magnetic resonance imaging (in vivo) was performed using an actively shielded Bruker 7.0 T BioSpin MRI scanner (Bruker Corp, Ettlingen, Germany), with B-GA20S gradient drivers and a 30 cm USR magnet. T₂-weighted morphological scans were performed using the Turbo RARE sequence with the following parameters: TR 4500 ms, TE 30 ms, FA 180.0 deg, TA 19min12s, FOV 32 × 32 mm, MTX 256 × 256. Angiography imaging angio-MRI TOF (time-of-flight) was performed using the FLASH sequence with the following parameters: TR 17 ms, TE 4.5 ms, FA 70 deg, TA 11 min6 s, FOV 32 × 32 mm, MTX 256 × 256.

Statistical analysis

Results are expressed as mean ± SD. The statistical significance of data was assessed using Student's t test and ANOVA test; $p < 0.05$ was considered statistically significant in all analyses. The Kaplan–Meier method was used to compare survival of animals in each group. All statistical analyses were performed using Statistica 13.3.

Results and discussion

In present study, the cytotoxic effects of nanoparticles subjected to an AMF were tested on A549 cell line using the Alamar Blue assay obtaining mean survival rates of 80% (14 mT), 66% (16 mT) and 21% (18 mT) presented in Fig. 1. As anticipated, elevating the magnetic induction value led to a proportional increase in cell mortality. Here, we found out that the use of magnetic induction at 18 mT gives a satisfactory outcome on reducing the viability of lung cancer cells, whereas control group, treated only with nanoparticles, maintained high viability. To date, the level of cell mortality exhibited variations

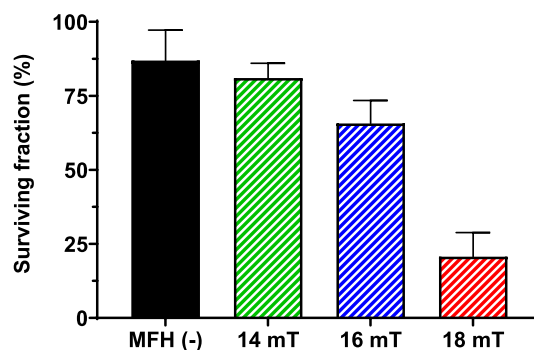


Fig. 1 Cytotoxic effects of iron oxide nanoparticles doped with magnesium on adenocarcinomic human alveolar basal epithelial cells (A549) treated with (14, 16, 18 mT) and without MFH(-) alternating magnetic fields. Data are mean \pm SD from three independent experiments ($n = 18$)

depending on the cell type, with certain cell populations showing a higher susceptibility to heat-induced effects than others, checked by other researchers (Armour et al. 1993; Labavić et al. 2020). A similar satisfactory cytotoxic effect due to MFH in in vitro models was also obtained by other scientists (Gao et al. 2010; Khandhar et al. 2012). Our research was confined to monolayer cell cultures, a model that might not precisely mirror the response of solid tumors to heating within a living organism. Past in vivo investigations have revealed a lower thermal threshold for tumor destruction when compared to cell cultures exposed to thermal conditions in vitro (Bhowmick et al. 2002; Tang et al. 2005), which, in conjunction with our results, offers promising prospects. Please note that scientists also compared the effects between hot-water hyperthermia (HWH) and MFH. As discussed by Rodríguez-Luccioni et al., in contrast to HWH, the MFH therapy using iron oxide nanoparticles led to a substantial decrease in cell viability, with observable variances dependent on the cell type in question (Rodríguez-Luccioni et al. 2011).

Following MFH treatments, the representative photographs were captured (displayed in the Supplementary Material, Figures S1-S3). These images allow for the observation of morphological characteristics of cells subjected to varying magnetic induction values. After the MFH treatment, the cells showed abnormal morphology and did not attach the culture plate in comparison to untreated cells which presented healthy appearance with high confluency. The largest number of unattached cells can be seen in photos after hyperthermia with 18 mT. The microscopic images captured under inverted microscopy clearly demonstrated that MFH caused notable changes in the morphology of A549 cells, and these changes were dependent on the magnetic induction strength. The treatment led to cell shrinkage, loss of epithelial features, and detachment from the substrate, all indicating cell death in correlation with higher magnetic induction levels. These changes are common for treating cells with increased temperature, as seen by other scientists (Haghniaz et al. 2015). The presented findings were substantiated through TEM studies, as shown in Fig. 2. These studies revealed an additional dimension, elucidating the accumulation of iron(III) oxide nanoparticles doped with magnesium within lung cancer cells. Notably, this accumulation was conspicuous across various cytoplasmic regions, resulting in the compromise of specific cellular structures, such as membranes, upon exposure to an AMF. Post a 24-h incubation period subsequent to exposure to the AMF,

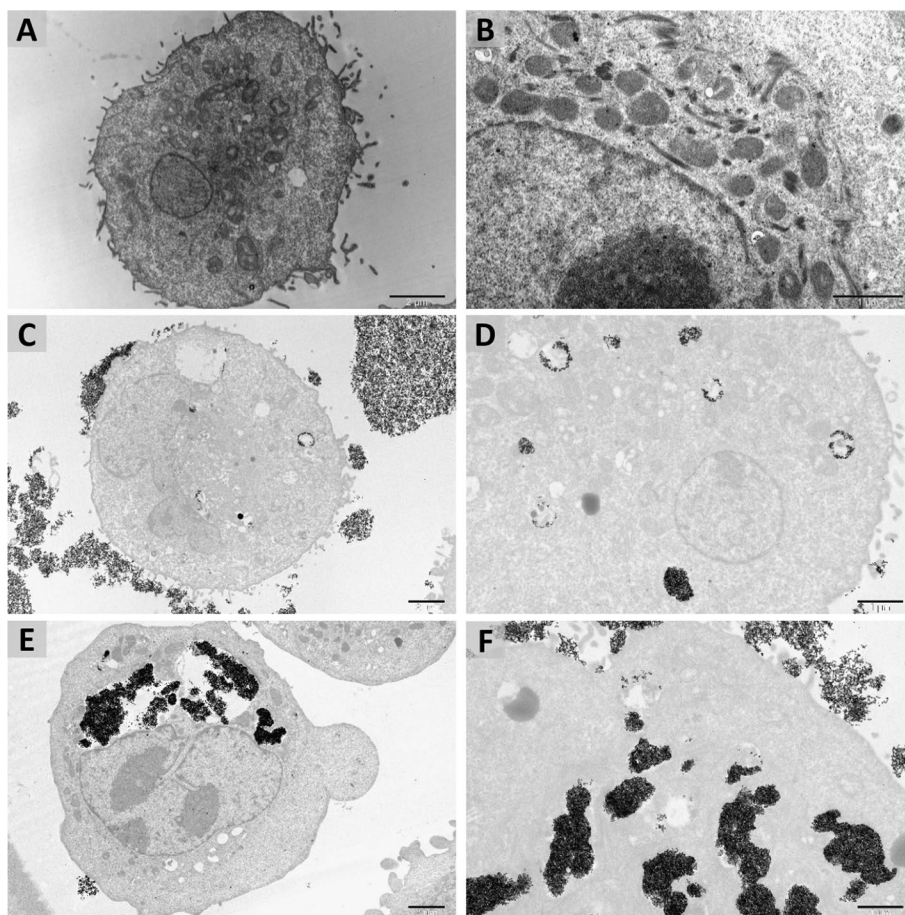


Fig. 2 Representative TEM images of adenocarcinomic human alveolar basal epithelial cells (A549) subjected to water ferrofluid ($0.250 \text{ mg}\cdot\text{mL}^{-1}$) composed of iron(III) oxide nanoparticles doped with magnesium and exposed without (**C** and **D**), and with alternating magnetic field (**E** and **F**). AMF: $B = 18 \text{ mT}$, $H_0 = 14.4 \text{ kA}\cdot\text{m}^{-1}$, $f = 110.1 \text{ kHz}$, current 11.04 A , voltage 26.92 V , capacitor 200 nF . The A549 cells exposed without AMF and treated without nanoparticles served as controls (**A** and **B**). Dark spots located in the cell and cell membrane as circular clusters are nanoparticles (**C**, **D**, **E**, **F**). Bar is $2 \mu\text{m}$ (**A**, **C**, **E**), bar is $1 \mu\text{m}$ (**B**, **D**, **F**)

a massive accumulation of nanoparticles was observed both inside and outside the lung cancer cell (Fig. 2E and F). In contrast, after a 24-h incubation period following exposure solely to nanoparticles (Fig. 2B and D), there was a significantly lower degree of accumulation compared to post-hyperthermia conditions. The observed morphological alterations, coupled with the decreased cell proliferation observed in the Alamar Blue assay, provide strong evidence for the potential anticancer efficacy of MFH using $\text{Mg}_{0.1}\text{-}\gamma\text{-Fe}_2\text{O}_3(\text{mPEG-silane})_{0.5}$ nanoparticles as a heat trigger if subject to an alternating magnetic field.

In the 1980s, during in vitro studies involving hyperthermia, attempts were made to investigate cell destruction kinetics based on the Arrhenius plot (Field and Morris 1983). The Arrhenius plot illustrates the relationship between the rate of inactivation in biological systems and temperature, with the logarithm of the inactivation rate plotted as a function of the reciprocal of absolute temperature. The Arrhenius Cell Damage Model (Chamani et al. 2023) treats cell death as a first-order chemical reaction, in which

living cells are transformed into dead ones. Based on the Arrhenius model, to facilitate the comparison of the heat sensitivity of different tissues, the “parameter” CEM43 (cumulative number of equivalent minutes at 43 °C) was developed to determine the thermal dose (Yung et al. 2010). The temperature of 43 °C was chosen as the reference point because it is representative for most human cells as the so-called break point in hyperthermia (Dewhirst et al. 2003a, b, c). The CEM43 parameter, initially introduced by Sapareto and Dewey in 1984 (Sapareto & Dewey 1984), quantifies the equivalent time in minutes at 43 degrees Celsius, a temperature often considered the threshold for cell viability, beyond which cells cease to be viable. In some articles (Mouratidis et al. 2019), the CEM43 parameter is denoted as TID (thermal isoeffective dose). The additional elaboration on this topic, along with the corresponding formulas, has been included in the Supplementary Material. As demonstrated in the 1980s, the susceptibility of cells to hyperthermia varies significantly. Note that the thermal sensitivity can vary greatly depending on the mammalian system and tissue type, even if they originate from the same organ. Rhoon et al. conducted an intriguing analysis of the utility of the CEM43 parameter, indicating that the TID with the CEM43 parameter does not directly predict cell survival after thermal exposure. Note that the TID thresholds depend on the specific tissue under investigation, the extent of damage, and the method used to assess the degree of injury (van Rhoon 2016a). Various tissues exhibit diverse responses to thermal stimuli; for instance, the tissues in the central nervous system are generally more sensitive to heat compared to other parts of the body (Haveman et al. 2005). In another study, it was demonstrated that human tissue exhibits greater thermal resistance compared to rodent tissue from similar organs, aligning with other findings in the literature, as discussed by Dewhirst et al. (Dewhirst et al. 2003a). The dosimetric unit CEM43 should serve solely as an indicator for determining the safe exposure time for tissue at any given temperature. Such results can be extrapolated to define iso-effect lines, but it has been shown that such application is appropriate only within the temperature range of 43.5 °C to 57 °C, as inaccuracies in extrapolation may occur at temperatures below or above this range (Dewhirst et al. 2003a). In summary, the challenge lies in precise and representative measurement of temperature distribution, especially in in vivo studies where there is heterogeneous blood flow within the tumor. The optimal approach would be to collect data from as many dimensions as possible to minimize result inaccuracies.

We presented the CEM43 results for three magnetic induction values in Table 2. In the CEM43 calculations, following the conventions of Sapareto and Dewey (1984),

Table 2 Results of the CEM43 value for magnetic fluid hyperthermia in lung cancer cells for three different magnetic induction values (14 mT, 16 mT, 18 mT), where S —mean cell survival probability, k —the cell injury rate, $CEM43$ —cumulative equivalent minutes

Magnetic induction value (B)	S	$k [s^{-1}]$	CEM43 [min] (calculated for $R_{CEM} = 0.25/0.5$)	CEM43 [min] (calculated for $R_{CEM} = 0.6579$)
14 mT	0.80	$8.32 \cdot 10^{-5}$	204.13	98.43
16 mT	0.66	$1.54 \cdot 10^{-4}$	1323.2	302.23
18 mT	0.21	$5.82 \cdot 10^{-4}$	10,509	1020.8

we assumed that R equals 0.5 for temperatures above 43 °C and 0.25 for temperatures below 43 °C. The constant R_{CEM} indicates how the heating time should be extended for temperatures below 43 °C and shortened for temperatures above 43 °C to achieve a biological effect equivalent to the equivalent heating for a specified time at 43 °C. In our study, with the increase in magnetic induction from 14 to 18 mT, a fourfold decrease in cell viability was observed, with the CEM43 parameter value increasing approximately 51 times. As the value of the magnetic field increases, the value of the parameter k —the cell injury rate increases. The calculated CEM43 values for the value of $R_{CEM}=0.6579$ are lower than for the value of $R_{CEM}=0.25/0.5$, because the higher the R_{CEM} value, the minutes of heating at a temperature above 43 °C are converted into a smaller number of equivalent minutes of heating at 43 °C. At the same time, the range of CEM43 values for extreme magnetic field values decreased.

The Arrhenius equation stands as a widely recognized empirical formula employed to delineate the temperature-driven variations in thermally induced processes. Specifically, this relationship finds common application in characterizing cell death concerning the interplay of temperature and the duration of hyperthermia treatments (Deckers et al. 2012). The determination of the $\ln(\Omega)$, the so-called tissue damage parameter, the values was employed in accordance with the assumed relationship with the inverse of absolute temperature on a scale of $1/T$ as given by equation (9) (please see the Supplementary Materials). The plot depicting the $\ln(\Omega)$ versus $1/T$ relationship, along with the fitted linear equation, is presented in Fig. 3A. Another way to determine E_a is to use the TID model and calculate the value based on the relationship $\ln(k)$ versus $1/T$ as given by equation (20) (please see the Supplementary Materials), presented in Fig. 3B.

Based on the calculated linear regression from the plot illustrating the relationship between $\ln(\Omega)$ and $1/T$, the kinetic parameters, activation energy (E_a) and frequency factor (A), were determined. In this work we considered $E_a=349.28 \text{ kJ}\cdot\text{mol}^{-1}$, and the frequency factor A took the value $2.6682\cdot 10^{53} \text{ s}^{-1}$. On the other hand, based on the calculated linear regression from the plot illustrating the relationship between $\ln(k)$ and $1/T$, we considered $E_a=349.25 \text{ kJ}\cdot\text{mol}^{-1}$, and the frequency factor A took the value $2.5483\cdot 10^{53} \text{ s}^{-1}$. The parameter values calculated for fitting the dependence of $\ln(\Omega)$ on $1/T$ are consistent with the values calculated for fitting the dependence of $\ln(k)$ on $1/T$. The determined values of the activation energy E_a and constant A are consistent with the data contained in the articles [18, 34]. For example, for the value of $A=2.6682\cdot 10^{53} \text{ s}^{-1}$, the E_a value calculated using formula (12) from article [18] is $348.36 \text{ kJ}\cdot\text{mol}^{-1}$, which is very close to the value of $349.28 \text{ kJ}\cdot\text{mol}^{-1}$ determined from the measurements. Based on formula (34), the $CEM43C_{1\%}$ value was calculated, i.e., the number of minutes needed to achieve cell survival of 1% at a temperature of 43 °C. The determined value, equal to 1477.0 min, is comparable to the results given in [18], e.g., to Rat RCC VX7 Cells data. For three S cell survival rates, 0.8, 0.66 and 0.21, taken from Table 2, $CEM43C_S$ was calculated, obtaining the following values: 65.027, 121.09 and 454.79. There is a better agreement between these values and the CEM43 values calculated for $R_{CEM}=0.6579$ than for $R_{CEM}=0.25/0.5$. With the determined activation energy value available, it can then be employed for the computation of the R_{CEM} parameter, as outlined in equation (23) (please see the Supplementary Materials). The R_{CEM} parameter calculated from equation (23) for the temperature $T=43 \text{ °C}$, a temperature often considered the

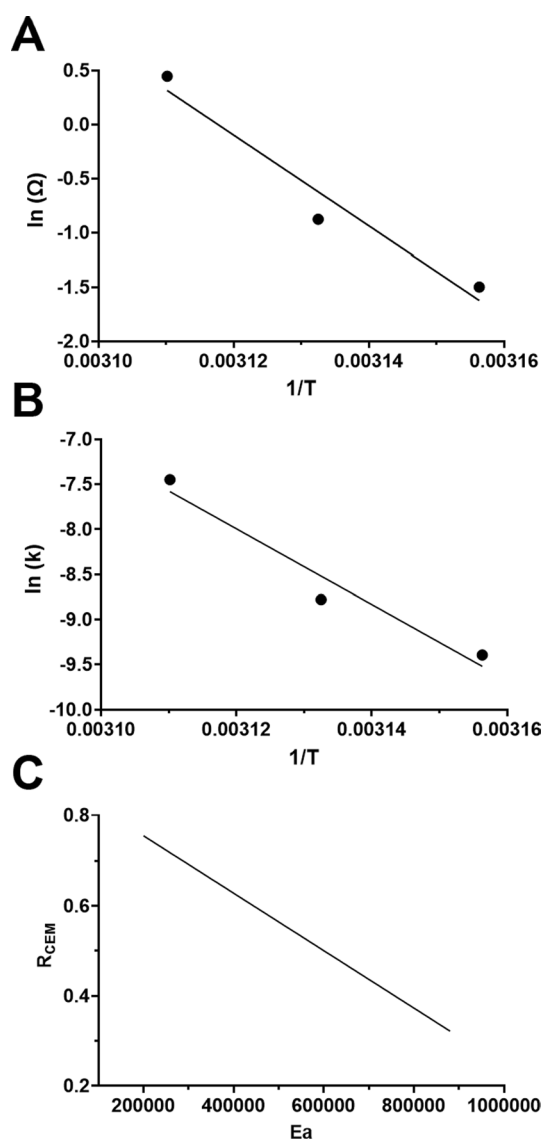


Fig. 3 Plots used for determination of activation energy and frequency factor: **A** the plot illustrating the relationship between the natural logarithm of the so-called tissue damage parameter [$\ln(\Omega)$] and the inverse of the temperature ($1/T$); **B** the plot illustrating the relationship between natural logarithm of the cell injury rate [$\ln(k)$] and the inverse of the temperature ($1/T$). **C** Theoretical dependence of R_{CEM} , a parameter used for CEM43 quantification, on the activation energy E_a [J·mol⁻¹] for temperature $T = 43$ °C, used next for determination of E_a value corresponding to R_{CEM} parameter value of 0.5

threshold for cell viability, is $R_{CEM} = 0.6579$. The obtained R_{CEM} , linked to the activation energy, can be employed for the computation of CEM43, as demonstrated in Table 2. The theoretical dependence of R_{CEM} on the activation energy E_a [J·mol⁻¹] was also calculated for the temperature $T = 43$ °C. Based on this, we could determine that the R_{CEM} parameter value of 0.5 is achieved at an activation energy of approximately 580 kJ·mol⁻¹. The graph, upon which this value was determined, is presented in Fig. 3C.

Values of activation energy determined by both methods, presented in Fig. 3A, B, differ by hundredths, but studies indicate that the TID model is a more conservative predictor of tissue damage at elevated temperatures compared to the Arrhenius model.

However, the Arrhenius model offers a more precise evaluation of tissue damage when contrasted with the TID model. Utilizing the TID model with a fixed R value of 0.5 is deemed unreliable and may lead to inaccuracies and errors in predictions (He et al. 2009; Mouratidis et al. 2019). For more precise predictions of thermal injuries and the determination of thermal thresholds, R_{CEM} , which is temperature and activation energy-dependent, should be utilized, as verified in the literature. Experiments conducted in vitro on hepatocellular carcinoma cells demonstrated that in the temperature spectrum of 50–60 °C, the R_{CEM} parameter can reach up to 0.72 (Reddy et al. 2013). Conversely, in prostate cells and tissues, this factor exhibits a range of values, fluctuating between 0.47 and 0.83 (He et al. 2009). Maintaining the parameter at a generic value of $R_{CEM}=0.25$ or 0.5 can significantly falsify the CEM43 results. In summary, the Arrhenius activation energy E_a obtained from experimental cell survival measurements can be utilized to calculate temperature-dependent R_{CEM} , providing a more accurate prediction of cell survival at high temperatures and thermal injury magnitudes.

In accordance with the Arrhenius law governing equilibrium thermodynamics, the rate of chemical reactions is correlated with temperature through activation energy. Consequently, the higher the activation energy, the slower the chemical reaction will be (Knapp and Huang 2022). According to the Eyring–Polanyi equation, E_a is related to the enthalpy of activation of the reaction, and A depends on the entropy of the reaction (Eyring 2004). The activation energy is generally described as “the reaction barrier” representing the energy required for the reaction to occur (Bickelhaupt and Houk 2017). In other words, the activation energy serves as the energy barrier for the formation of the critical transition state during the rate-limiting inactivation step. Metabolic reactions and other enzymatic processes exhibit relatively low activation energies, typically ranging from 3 to 20 kcal/mol, whereas thermal damage is associated with substantially higher activation energies, within the range of 100 to 200 kcal/mol (Lepock 2003). The elevated activation energy indicates that during the cell-killing process in hyperthermia, there is a significant transition occurring either within the macromolecule or the cellular structure, imposing a constraint on the rate of this cell destruction. Westra and Dewey proposed that the elevated activation energy at the level of 200 kcal/mol associated with hyperthermic cell killing indicates that the rate-limiting step is the denaturation of proteins (Westra and Dewey 1971). Activation energy is typically highly diverse depending on cell type and tissues. Additionally, it has been noted that attempts have been made to use higher-order kinetic models to describe thermal damage, assuming the existence of one or more intermediate states between the viable and dead states, although the first-order kinetic model is most appropriate for most situations (Dienes 1966). The derived kinetic parameters can be valuable in developing hyperthermic strategies and are often incorporated into theoretical simulations concerning the temperature increase within tumor masses (Marissa Nichole et al. 2006; Rylander et al. 2010). Other studies report the activation energy for thermal damage studies (Singh et al. 2020; Westra and Dewey 1971) and thermal protein denaturation (Qin et al. 2014) at a similar level to that obtained in the presented studies.

In cell culture studies, the breakpoint of cell threshold temperature above which cells are no longer viable and/or seriously damaged is around 43 °C or above. This was confirmed in our present studies with lung cancer cells (in vitro) exposed to an AMF.

Note that the thermal damage to the tissues depends upon several factors. For example, temperature elevation and duration of thermal exposure are two major factors that determine the thermogenesis for a particular tissue. How these factors affect human lung cancer tissues was further studied using a preclinical xenograft model. In our studies, MFH was tested in BALB/c nude mice bearing human lung A549 cancer in a solid tumor. Before each magnetization, the animals were injected intratumorally with a single dose of magnesium-doped iron(III) oxide nanoparticle and further subjected to an AMF. Referring to the standard protocols proposed for magnetic fluid hyperthermia in some clinical studies (Herrero de la Parte et al. 2022), we performed four separate magnetization sessions with seven days intervals before each new magnetization. The first magnetic hyperthermia was started on day 14th post-implantation of lung cancer cells into right flank in mice revealing for this day a similar tumor size across all implanted animals ($2.9 \pm 1.2 \text{ mm}^3$ in control group vs $2.1 \pm 1.5 \text{ mm}^3$ in AMF-treated group, with $p < 0.05$). In the performed study, both treated and non-treated animals were routinely inspected on weekly intervals for general health conditions including measuring body weight gain and tumor sizes (Fig. 4A, C). In the control mice bearing lung cancers not subjected to MFH the body weight gain was much faster than body weight gain observed in hyperthermia-treated animals (Fig. 4A). This was also accompanied with larger tumor volumes reaching much faster a critical size value, which is used as a check point to exclude the animal from the study (Fig. 4B). In the experimental setup, mice with tumor sizes exceeding 12 mm in at least one direction were excluded from the study due to animal welfare regulation. In this way, two control (non-treated) mice were excluded on day 28th post-treatment and one hyperthermia-treated mouse was excluded on day 35th post-treatment (Fig. 4B). As shown in Fig. 4B, the rest of the control (non-treated) mice were excluded from the study on day 35th due to exceeded tumor size. No further exclusion was performed for other treated animals subjected to MFH. No mortality was also observed in this group. The experiment was terminated one week after the last MFH, however, no animals were found to be excluded due to the tumor size on this date. Studies evidenced that mice subjected to magnetic hyperthermia showed a significant tumor-growth suppression ($V = 169 \pm 94 \text{ mm}^3$; $p < 0.05$) compared to the control non-treated mice (Fig. 4C). The representative photographs of the tumors resected from the mice in each group on the day when each individual mouse was excluded from the experiment are shown in Fig. 4D. Moreover, the AMF-exposed animals also exhibited slower tumor growth in the experimental period. Note that MFH-induced thermal effects were considered to improve the significant regression of the tumor size in MFH-treated mice. This was also evidenced on magnetic resonance imaging (MRI) showing the tumor and its vasculature on T2-weighted and MRI-TOF images (Fig. 5). Note that iron(III) oxide nanoparticles doped with magnesium strongly diminished signal intensities resulting in a large darkening on T2-weighted images. More details on relaxometry measurements of these nanoparticles are shown in Supplementary Material (Figure S4).

In the hyperthermia studies, we applied infrared (IR) imaging using a thermal IR camera to determine a temperature profile of the tumor in magnetized mice (Fig. 4E). When mice were injected with nanoparticles and exposed to an AMF, the temperature at the tumor site increased up to ca. $43 \text{ }^\circ\text{C}$ (Fig. 4E). Therefore, the magnetization

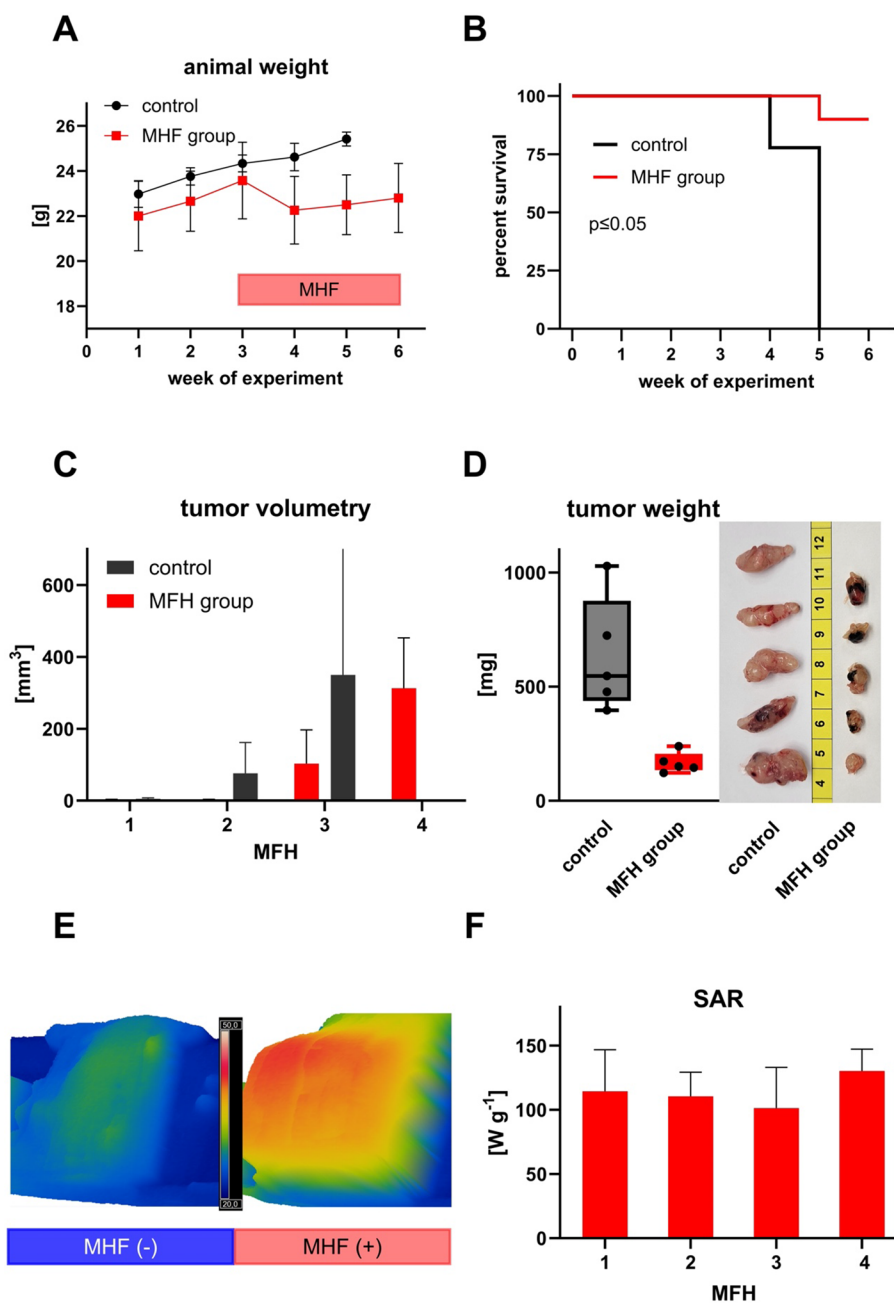


Fig. 4 Therapeutic efficacy of MFH in human lung cancer xenograft NUDE Balb/c mice exposed to an alternating magnetic field and iron(III) oxide nanoparticles doped with magnesium. **A** Animal weight gain in the experiment; **B** Kaplan–Meier survival analysis; **C** tumor volume assessed on the selected treatment day; **D** tumor mass and representative photographs of the tumors taken post-mortem from the mice on the day, which the mice were excluded from the experiment; **E** representative infrared images of temperature distribution in the tumor before MFH (left panel) and 15 min of MFH (right panel); **F** SAR values expressed as mean \pm SD for xenografts ($W \cdot g^{-1}$ of NPs)

setup for animal studies was lower than the Hergt and Dutz limit ($5 \cdot 10^9 \text{ A} \cdot \text{m}^{-1} \cdot \text{s}^{-1}$) approved for biological safety in humans (Hergt & Dutz 2007; Vicentini et al. 2022). Furthermore, it is worth noting that tumor cells generally have a higher susceptibility to heat due to their distinct physiology and microenvironment. Tumors often possess

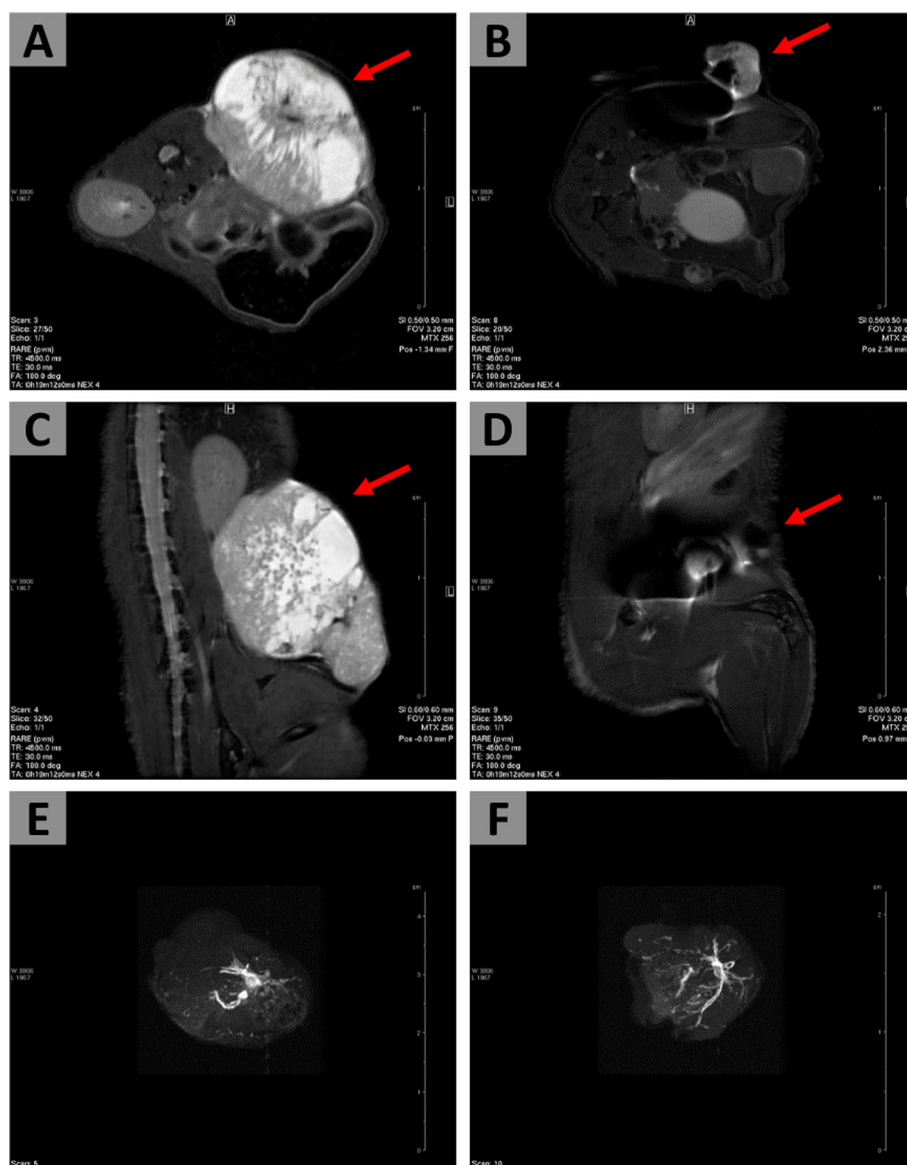


Fig. 5 Representative anatomy and angiography images of NUDE Balb/c mice bearing human lung cancer (A549). Mice were treated with (B, D, F) or without (A, C, E) MFH. In MFH-treated mice, the animals were intratumorally injected (0.2 mL) with $\text{Mg}_{0.1}\text{-}\gamma\text{-Fe}_2\text{O}_3(\text{mPEG-silane})_{0.5}$ nanoparticles ($3 \text{ mg}\cdot\text{mL}^{-1}$) and subjected to an AMF for 30 min (B 23 mT, H_0 $18.3 \text{ kA}\cdot\text{m}^{-1}$, f 110.1 kHz). Non-treated mice were served as controls (please see the experiment section). T2-weighted anatomy scans (A–D) was performed using the Turbo RARE sequence (TR 4500 ms, TE 30 ms, FA 180.0 deg, TA 19 min12 s, FOV $32 \times 32 \text{ mm}$, MTX 256×256) in the axial (A, B) and coronal (C, D) plane. Angiography imaging (E, F) angio-MRI TOF (time-of-flight) was performed using the FLASH sequence with the following parameters: TR 17 ms, TE 4.5 ms, FA 70 deg, TA 11 min6s, FOV $32 \times 32 \text{ mm}$, MTX 256×256

an abnormal blood supply that is less efficient at dispersing heat compared to normal tissue. This inefficiency leads to elevated localized temperatures within the tumor during hyperthermia treatment. Additionally, tumor cells have higher metabolic rates and typically exist in a more acidic and hypoxic environment, rendering them more vulnerable to heat stress (Amissah et al. 2024; Song 1984). In animals, a potent harm

was only found under conditions of exposure characterized by a whole-body average SAR substantially higher than $4 \text{ W}\cdot\text{kg}^{-1}$; this value can be assumed as a threshold below which adverse effects would not be expected (Osepchuk and Petersen 2003). In recent studies, magnetic nanoclusters consisting of SPION cores doped with zinc/manganese or cobalt/manganese were demonstrated to be used as heat mediators for MFH because of their high heating efficiency and controllable temperature functionality (Albarqi et al. 2020, 2019). Iron(III) oxide nanoparticles doped with magnesium used in the present study has attracted much interest because the concentration of these nanoparticles was sufficient to generate the SAR value allowing the efficient ablation of lung cancer tissues. The SAR values calculated based on the tumor temperature measured for each individual hyperthermia session are shown in Fig. 4F. The obtained data highlight the superior in vivo heating efficiency of iron(III) oxide nanoparticles doped with magnesium if the local nanoparticle concentration is achieved to generate the proper SAR values in the tumor. In animal studies, the nanoparticles at the concentration of $3 \text{ mg}\cdot\text{mL}^{-1}$ were used in hyperthermia experiments using AMF at the strength field of $18.3 \text{ kA}\cdot\text{m}^{-1}$ and fixed frequency of 110.1 kHz. With the available temperature history within the tumor tissue, it is then possible to determine whether the temperature reach sufficient levels to cause injury and whether those levels are sustained for a sufficiently long-term duration. To assess the potential of MFH for cancer injury in case of a low-level but long duration thermal exposures, the cumulative thermal exposure method was applied (Dewhirst et al. 2003a, 2003b; Viglianti et al. 2014; Yarmolenko et al. 2011). According to this method the value of R_{CEM} is 0.25 at temperatures below $43.0 \text{ }^\circ\text{C}$, while above $43.0 \text{ }^\circ\text{C}$ value of R_{CEM} is 0.5. On this basis, the average value of CEM43 was calculated for 9.6 min for all MFH sessions applied on mice bearing human lung A549 cancer. According to van Rhoon et al. the lowest thermal dose resulting in tissue damages for a mouse is 3.4 CEM43 (van Rhoon et al. 2013). The literature indicates that elevating tissue temperature to $39\text{--}40 \text{ }^\circ\text{C}$ can enhance tumor blood flow and microcirculation. As temperature rises beyond this range, tumor perfusion continues to increase until reaching a threshold thermal dose, leading to a subsequent decrease in tumor blood flow. Notably, there is a noted threshold of $39 \text{ }^\circ\text{C}$ for extravasation, and temperatures between 40 and $42 \text{ }^\circ\text{C}$ are associated with increased nanoparticle extravasation (van Rhoon et al. 2020; Viglianti et al. 2014; Vujaskovic et al. 2010). The average CEM43 value achieved in our preclinical hyperthermia studies on lung cancer is higher than those which cause damages to mice tissue.

The MFH of tumor involves directly injection of magnetic nanoparticles into the tumor to generate heat due to an AMF. This method has some advantages regarding the accuracy, targeting, and temperature control and avoids overheating the normal tissues around the tumor (Johannsen et al. 2010). High temperature can destroy the biological integrity of the cell membrane and increase its permeability, which is conducive to the penetration and absorption of chemical drugs and gene transfer. The interior of solid tumors is often anoxic due to vascular disorder, while the anoxic cancer cells are usually acidic and nutrient-poor, making them more vulnerable to heat damage. Studies evidence that high temperature can temporarily improve the oxygen and blood supply to the tumor helping drugs to enter the tumor and improving the radiation susceptibility of tumor cells (Lu et al. 2020; van Rhoon 2016b). Therefore, MFH is a promising treatment

for tumors, and it should be further tested as a stand-alone treatment and/or adjuvant approach with chemo- or radiotherapy (Vaupel & Kelleher 2012; Westermann et al. 2012).

In summary, the challenges of MFH extend beyond creating suitable nanoparticles (biocompatible, non-toxic, and generating high SAR in AMF) for therapeutic use. It also involves a thorough understanding of their mechanisms of action and the effects they induce. Only then is there a chance for successfully designing and optimizing the protocol for this kind of treatment. This is particularly crucial in the context of regulatory approval, which necessitates demonstrating the efficacy and safety of the nanoparticles through rigorous preclinical and clinical trials. Notably, MagForce's NanoTherm therapy stands as the foremost and sole nanotechnology-driven treatment endorsed by European regulatory authorities (Mahmoudi et al. 2018). Moreover, addressing the production scalability and ensuring consistent quality and reproducibility of the nanoparticles are essential steps for clinical translation. The development of standardized operating procedures and quality control measures will help in meeting regulatory requirements. Collaboration between researchers, clinicians, and regulatory bodies is vital to streamline the transition from laboratory research to clinical application. By overcoming these multifaceted challenges, MFH has the potential to become a valuable addition to the arsenal of cancer therapies (Liu et al. 2020; Rubia-Rodríguez et al. 2021).

Conclusions

We performed magnetic fluid hyperthermia studies on human lung cancer cells (in vitro) and NUDE mice bearing human lung cancer (in vivo) treated with newly synthesized magnesium-doped iron(III) oxide nanoparticles subjected to an alternating magnetic field with different strength fields. The magnetization setups for both cellular and animal experiments were performed below the Hergt and Dutz limit, which is recognized as a safety threshold for biological investigations. Here, we observed that the lung cancer cells treated with nanoparticles and magnetized for $14.4 \text{ kA}\cdot\text{m}^{-1}$ yielded a satisfactory outcome in reducing the viability up to ca. 21% (in vitro). Because the activation energy tends to exhibit considerable variability contingent upon the cell type and/or tissues, the energy for lung cancer cells was calculated for $349 \text{ kJ}\cdot\text{mol}^{-1}$, which aligns comparably with levels of the activation energy observed in other hyperthermia in vitro studies. In our study, we also emphasize how the activation energy is correlated with the R_{CEM} parameter, which constitutes a component of the formula necessary for calculating the thermal dose threshold, the CEM43 parameter. We highlight that adopting a generally assumed R_{CEM} of 0.5 for $T > 43 \text{ }^\circ\text{C}$ and 0.25 for $T < 43 \text{ }^\circ\text{C}$ can lead to significant inaccuracies in the actual CEM43 result. Note that CEM43 values for in vitro studies are of entirely different orders of magnitude than those obtained for in vivo studies, and they cannot be directly compared. To further address the question of how the thermal energy introduced into the lung cancer cells impacts overall the tumor burden in solid tissues, we performed animal studies using BALB/c NUDE mice as models. It was found that MFH due to an AMF ($18.3 \text{ kA}\cdot\text{m}^{-1}$) and magnesium-doped iron(III) oxide nanoparticles dosed intratumorally exhibited excellent anticancer efficacies in mice bearing human lung cancer cells. The CEM43 value for this treatment was estimated for ca. 9.6 min with the SAR level ranging from 100 to $150 \text{ W}\cdot\text{g}^{-1}$. In conclusion, the satisfactory outcomes

from the preclinical studies using cellular (in vitro) and murine (in vivo) models indicate a notable efficient anticancer effect of magnetic fluid hyperthermia induced with magnesium-doped iron(III) oxide nanoparticles subjected to an alternating magnetic field. Considering all of these data, the proposed magnetic fluid hyperthermia as a novel strategy for lung cancer therapy remains a promising new therapeutic approach for a stand-alone treatment in human lung cancer.

Supplementary Information

The online version contains supplementary material available at <https://doi.org/10.1186/s12645-024-00276-0>.

Additional file 1.

Acknowledgements

The authors are grateful to Michal Wieteska and Marlena Welniak-Kaminska for their support in preclinical MRI studies.

Author contributions

Conceptualization, M.S. and I.P.G.; methodology, M.S., G.D.; investigation, M.S., G.D, M.B.K., A.K.; resources, M.S.; data curation, M.S., G.D.; writing—original draft preparation, M.S., I.P.G.; writing—review and editing, M.S., G.D, M.B.K., A.K., A.N., M.R.A., I.P.G.; visualization, M.S.; supervision, I.P.G.; project administration, I.P.G.; funding acquisition I.P.G.

Funding

The work was financially supported by the Programme “Applied Research” through TEPCAN project granted under the Norwegian Financial Mechanisms 2014–2021 / POLNOR 2019 (EEA and Norway Grants), Thematic areas: Welfare, health and care (NCBR Funding No. NOR/POLNOR/TEPCAN/0057/2019-00).

Availability of data and materials

No datasets were generated or analysed during the current study.

Declarations

Ethics approval and consent to participate

No human participants, human data or human tissue were involved in this study. All animal experiments were carried out in accordance with the consent of the Local Ethical Committee for Experiments on Animals (Uchwala nr WAW2/077/2022).

Consent for publication

All authors read and approved the final version of the manuscript.

Competing interests

The authors declare no competing interests.

Received: 13 May 2024 Accepted: 16 July 2024

Published online: 22 July 2024

References

- Albarqi HA, Wong LH, Schumann C, Sabei FY, Korzun T, Li XN, Hansen MN, Dhagat P, Moses AS, Taratula O, Taratula O (2019) Biocompatible nanoclusters with high heating efficiency for systemically delivered magnetic hyperthermia. *ACS Nano* 13(6):6383–6395. <https://doi.org/10.1021/acsnano.8b06542>
- Albarqi HA, Demessie AA, Sabei FY, Moses AS, Hansen MN, Dhagat P, Taratula OR, Taratula O (2020) Systemically delivered magnetic hyperthermia for prostate cancer treatment. *Pharmaceutics* 12(11):1020. <https://doi.org/10.3390/pharmaceutics12111020>
- Altintas G, Akduman I, Janjic A, Yilmaz T (2021) A novel approach on microwave hyperthermia. *Diagnostics* (basel). <https://doi.org/10.3390/diagnostics11030493>
- Amisshah HA, Combs SE, Shevtsov M (2024) Tumor dormancy and reactivation: the role of heat shock proteins. *Cells* 13(13):1087
- Armour EP, McEachern D, Wang Z, Corry PM, Martinez A (1993) Sensitivity of human cells to mild hyperthermia1. *Can Res* 53(12):2740–2744
- Bhowmick S, Hoffmann NE, Bischof JC (2002) Thermal therapy of prostate tumor tissue in the dorsal skin flap chamber. *Microvasc Res* 64(1):170–173. <https://doi.org/10.1006/mvre.2002.2408>
- Bickelhaupt FM, Houk KN (2017) Analyzing reaction rates with the distortion/interaction-activation strain model. *Angew Chem Int Ed Engl* 56(34):10070–10086. <https://doi.org/10.1002/anie.201701486>
- Brollo MEF, Pinheiro IF, Bassani GS, Varet G, Guersoni VCB, Knobel M, Bannwart AC, Muraca D, van der Geest C (2021) Iron oxide nanoparticles in a dynamic flux: implications for magnetic hyperthermia-controlled fluid viscosity. *ACS Appl Nano Mater* 4(12):13633–13642. <https://doi.org/10.1021/acsnm.1c03061>

- Catherine CB, Adam SGC (2003) Functionalisation of magnetic nanoparticles for applications in biomedicine. *J Phys D Appl Phys* 36(13):R198. <https://doi.org/10.1088/0022-3727/36/13/203>
- Chamani F, Pyle MM, Shrestha TB, Sebek J, Bossmann SH, Basel MT, Sheth RA, Prakash P (2023) In vitro measurement and mathematical modeling of thermally-induced injury in pancreatic cancer cells. *Cancers* 15(3):655
- Deckers R, Debeissat C, Fortin PY, Moonen CT, Couillaud F (2012) Arrhenius analysis of the relationship between hyperthermia and Hsp70 promoter activation: a comparison between ex vivo and in vivo data. *Int J Hyperthermia* 28(5):441–450. <https://doi.org/10.3109/02656736.2012.674620>
- Dewhirst MW, Viglianti BL, Lora-Michiels M (2003a) Thermal dose requirement for tissue effect: experimental and clinical findings. Proceedings of SPIE [Thermal treatment of tissue: Energy delivery and assessment ii]. Conference on Thermal Treatment of Tissue: Energy Delivery and Assessment II, San Jose, Ca
- Dewhirst MW, Viglianti BL, Lora-Michiels M, Hanson M, Hoopes PJ (2003b) Basic principles of thermal dosimetry and thermal thresholds for tissue damage from hyperthermia. *Int J Hyperthermia* 19(3):267–294. <https://doi.org/10.1080/0265673031000119006>
- Dewhirst MW, Viglianti BL, Lora-Michiels M, Hoopes PJ, Hanson M (2003c) Thermal dose requirement for tissue effect: experimental and clinical findings. *Proc SPIE Int Soc Opt Eng* 4954:37. <https://doi.org/10.1117/12.476637>
- Diederich CJ, Hynynen K (1999) Ultrasound technology for hyperthermia. *Ultrasound Med Biol* 25(6):871–887. [https://doi.org/10.1016/S0301-5629\(99\)00048-4](https://doi.org/10.1016/S0301-5629(99)00048-4)
- Dienes GJ (1966) A kinetic model of biological radiation response. *Radiat Res* 28(2):183–202
- Eyring H (2004) The activated complex in chemical reactions. *J Chem Phys* 3(2):107–115. <https://doi.org/10.1063/1.1749604>
- Fan W, Yung B, Huang P, Chen X (2017) Nanotechnology for multimodal synergistic cancer therapy. *Chem Rev* 117(22):13566–13638. <https://doi.org/10.1021/acs.chemrev.7b00258>
- Field SB, Morris CC (1983) The relationship between heating time and temperature: its relevance to clinical hyperthermia. *Radiother Oncol* 1(2):179–186. [https://doi.org/10.1016/S0167-8140\(83\)80020-6](https://doi.org/10.1016/S0167-8140(83)80020-6)
- Gao F, Cai Y, Zhou J, Xie X, Ouyang W, Zhang Y, Wang X, Zhang X, Wang X, Zhao L, Tian T (2010) Pullulan acetate coated magnetite nanoparticles for hyper-thermia: preparation, characterization and in vitro experiments. *Nano Res* 3:23–31. <https://doi.org/10.1007/s12274-010-1004-6>
- Habash RW, Bansal R, Krewski D, Alhafid HT (2006) Thermal therapy, part 2: hyperthermia techniques. *Crit Rev Biomed Eng* 34(6):491–542. <https://doi.org/10.1615/critrevbiomedeng.v34.i6.30>
- Haghniaz R, Umrani RD, Paknikar KM (2015) Temperature-dependent and time-dependent effects of hyperthermia mediated by dextran-coated La_{0.7}Sr_{0.3}MnO₃: in vitro studies. *Int J Nanomedicine* 10:1609–1623. <https://doi.org/10.2147/ijn.S78167>
- Haveman J, Sminia P, Wondergem J, van der Zee J, Hulshof MC (2005) Effects of hyperthermia on the central nervous system: what was learnt from animal studies? *Int J Hyperthermia* 21(5):473–487. <https://doi.org/10.1080/02656730500159079>
- He X, Bhowmick S, Bischof JC (2009) Thermal therapy in urologic systems: a comparison of arrhenius and thermal isoeffective dose models in predicting hyperthermic injury. *J Biomech Eng*. <https://doi.org/10.1115/1.3128671>
- Hergt R, Dutz S (2007) Magnetic particle hyperthermia-biophysical limitations of a visionary tumour therapy. *J Magn Magn Mater* 311(1):187–192. <https://doi.org/10.1016/j.jmmm.2006.10.1156>
- Hergt R, Dutz S, Müller R, Zeisberger M (2006) Magnetic particle hyperthermia: nanoparticle magnetism and materials development for cancer therapy. *J Phys: Condens Matter* 18(38):S2919. <https://doi.org/10.1088/0953-8984/18/38/S26>
- Herrero de la Parte B, Rodrigo I, Gutiérrez-Basoa J, Iturrizaga Correcher S, Mar Medina C, Echevarría-Uraga JJ, García JA, Plazaola F, García-Alonso I (2022) Proposal of new safety limits for in vivo experiments of magnetic hyperthermia antitumor therapy. *Cancers (basel)*. <https://doi.org/10.3390/cancers14133084>
- Hirata E, Sahai E (2017) Tumor microenvironment and differential responses to therapy. *Cold Spring Harb Perspect Med*. <https://doi.org/10.1101/cshperspect.a026781>
- Jaeger S, Duran-Frigola M, Aloy P (2015) Drug sensitivity in cancer cell lines is not tissue-specific. *Mol Cancer* 14(1):40. <https://doi.org/10.1186/s12943-015-0312-6>
- Jamal-Hanjani M, Quezada SA, Larkin J, Swanton C (2015) Translational implications of tumor heterogeneity. *Clin Cancer Res* 21(6):1258–1266. <https://doi.org/10.1158/1078-0432.Ccr-14-1429>
- Jang J-T, Lee J, Seon J, Ju E, Kim M, Kim YI, Kim MG, Takemura Y, Arbab AS, Kang KW, Park KH, Paek SH, Bae S (2018) Giant magnetic heat induction of magnesium-doped γ -Fe₂O₃ superparamagnetic nanoparticles for completely killing tumors. *Adv Mater* 30(6):1704362. <https://doi.org/10.1002/adma.201704362>
- Johannsen M, Thiesen B, Wust P, Jordan A (2010) Magnetic nanoparticle hyperthermia for prostate cancer. *Int J Hyperthermia* 26(8):790–795. <https://doi.org/10.3109/02656731003745740>
- Jordan A, Scholz R, Wust P, Fähling H, Roland F (1999) Magnetic fluid hyperthermia (MFH): cancer treatment with AC magnetic field induced excitation of biocompatible superparamagnetic nanoparticles. *J Magn Magn Mater* 201(1):413–419. [https://doi.org/10.1016/S0304-8853\(99\)00088-8](https://doi.org/10.1016/S0304-8853(99)00088-8)
- Khandhar AP, Ferguson RM, Simon JA, Krishnan KM (2012) Tailored magnetic nanoparticles for optimizing magnetic fluid hyperthermia. *J Biomed Mater Res A* 100(3):728–737. <https://doi.org/10.1002/jbm.a.34011>
- Knapp BD, Huang KC (2022) The effects of temperature on cellular physiology. *Annu Rev Biophys* 51:499–526. <https://doi.org/10.1146/annurev-biophys-112221-074832>
- Kozissnik B, Bohorquez AC, Dobson J, Rinaldi C (2013) Magnetic fluid hyperthermia: advances, challenges, and opportunity. *Int J Hyperthermia* 29(8):706–714. <https://doi.org/10.3109/02656736.2013.837200>
- Kumar CS, Mohammad F (2011) Magnetic nanomaterials for hyperthermia-based therapy and controlled drug delivery. *Adv Drug Deliv Rev* 63(9):789–808. <https://doi.org/10.1016/j.addr.2011.03.008>
- Labavić D, Ladžimi MT, Courtade E, Pfeuty B, Thommen Q (2020) Mammalian cell sensitivity to hyperthermia in various cell lines: a new universal and predictive description. *Int J Hyperthermia* 37(1):506–516. <https://doi.org/10.1080/02656736.2020.1762005>

- Lepock JR (2003) Cellular effects of hyperthermia: relevance to the minimum dose for thermal damage. *Int J Hypertherm* 19(3):252–266. <https://doi.org/10.1080/0265673031000065042>
- Liu X, Zhang Y, Wang Y, Zhu W, Li G, Ma X, Zhang Y, Chen S, Tiwari S, Shi K, Zhang S, Fan HM, Zhao YX, Liang XJ (2020) Comprehensive understanding of magnetic hyperthermia for improving antitumor therapeutic efficacy. *Theranostics* 10(8):3793–3815. <https://doi.org/10.7150/thno.40805>
- Lu CH, Hsiao JK (2023) Diagnostic and therapeutic roles of iron oxide nanoparticles in biomedicine. *Tzu Chi Med J* 35(1):11–17. https://doi.org/10.4103/tcmj.tcmj_65_22
- Lu Y, Rivera-Rodriguez A, Tay ZW, Hensley D, Fung KLB, Colson C, Saayujya C, Huynh Q, Kabuli L, Fellows B, Chandrasekharan P, Rinaldi C, Conolly S (2020) Combining magnetic particle imaging and magnetic fluid hyperthermia for localized and image-guided treatment. *Int J Hypertherm* 37(3):141–154. <https://doi.org/10.1080/02656736.2020.1853252>
- Mahmoudi K, Bouras A, Bozec D, Ivkov R, Hadjipanayis C (2018) Magnetic hyperthermia therapy for the treatment of glioblastoma: a review of the therapy's history, efficacy and application in humans. *Int J Hypertherm* 34(8):1316–1328. <https://doi.org/10.1080/02656736.2018.1430867>
- Mantso T, Vasileiadis S, Anestopoulos I, Voulgaridou GP, Lampri E, Botaitis S, Kontomanolis EN, Simopoulos C, Goussetis G, Franco R, Chlichlia K, Pappa A, Panayiotidis MI (2018) Hyperthermia induces therapeutic effectiveness and potentiates adjuvant therapy with non-targeted and targeted drugs in an in vitro model of human malignant melanoma. *Sci Rep* 8(1):10724. <https://doi.org/10.1038/s41598-018-29018-0>
- Marissa Nichole R, Yusheng F, Yongjie Z, Jon B, Roger Jason S, Andrei V, John DH, Kenneth RD (2006) Optimizing heat shock protein expression induced by prostate cancer laser therapy through predictive computational models. *J Biomed Opt* 11(4):041113. <https://doi.org/10.1117/1.2241310>
- Marusyk A, Polyak K (2010) Tumor heterogeneity: causes and consequences. *Biochimica Et Biophysica Acta BBA Reviews on Cancer* 1805(1):105–117. <https://doi.org/10.1016/j.bbcan.2009.11.002>
- Mouratidis PXE, Rivens I, Civale J, Symonds-Taylor R, ter Haar G (2019) Relationship between thermal dose and cell death for "rapid" ablative and "slow" hyperthermic heating. *Int J Hypertherm* 36(1):228–242. <https://doi.org/10.1080/02656736.2018.1558289>
- Nowicka AM, Ruzicka-Ayoush M, Kasprzak A, Kowalczyk A, Bamburowicz-Klimkowska M, Sikorska M, Sobczak K, Donten M, Ruszczynska A, Nowakowska J, Grudzinski IP (2023) Application of biocompatible and ultrastable superparamagnetic iron(iii) oxide nanoparticles doped with magnesium for efficient magnetic fluid hyperthermia in lung cancer cells. *J Mater Chem B* 11(18):4028–4041. <https://doi.org/10.1039/D3TB00167A>
- Obaidat IM, Narayanaswamy V, Alaabed S, Sambasivam S, Muralee Gopi CVV (2019) Principles of magnetic hyperthermia: a focus on using multifunctional hybrid magnetic nanoparticles. *Magnetochemistry* 5(4):67
- Oliveira TR, Stauffer PR, Lee CT, Landon CD, Etienne W, Ashcraft KA, McNerny KL, Mashal A, Nouls J, Maccarini PF, Beyer WF Jr, Inman B, Dewhirst MW (2013) Magnetic fluid hyperthermia for bladder cancer: a preclinical dosimetry study. *Int J Hyperthermia* 29(8):835–844. <https://doi.org/10.3109/02656736.2013.834384>
- Osepchuk JM, Petersen RC (2003) Historical review of RF exposure standards and the International Committee on Electromagnetic Safety (ICES). *Bioelectromagnetics*. <https://doi.org/10.1002/bem.10150>
- Qin Z, Balasubramanian SK, Wolkers WF, Pearce JA, Bischof JC (2014) Correlated parameter fit of Arrhenius model for thermal denaturation of proteins and cells. *Ann Biomed Eng* 42(12):2392–2404. <https://doi.org/10.1007/s10439-014-1100-y>
- Rampersad SN (2012) Multiple applications of alamar blue as an indicator of metabolic function and cellular health in cell viability bioassays. *Sensors* 12(9):12347–12360. <https://doi.org/10.3390/s120912347>
- Reddy G, Dreher MR, Rossmann C, Wood BJ, Haemmerich D (2013) Cytotoxicity of hepatocellular carcinoma cells to hyperthermic and ablative temperature exposures: in vitro studies and mathematical modelling. *Int J Hypertherm* 29(4):318–323
- Rodrigues HF, Capistrano G, Bakuzis AF (2020) In vivo magnetic nanoparticle hyperthermia: a review on preclinical studies, low-field nano-heaters, noninvasive thermometry and computer simulations for treatment planning. *Int J Hypertherm* 37(3):76–99. <https://doi.org/10.1080/02656736.2020.1800831>
- Rodríguez-Luccioni HL, Latorre-Esteves M, Méndez-Vega J, Soto O, Rodríguez AR, Rinaldi C, Torres-Lugo M (2011) Enhanced reduction in cell viability by hyperthermia induced by magnetic nanoparticles. *Int J Nanomed* 6:373–380. <https://doi.org/10.2147/IJN.S14613>
- Rubia-Rodríguez I, Santana-Otero A, Spassov S, Tombácz E, Johansson C, De La Presa P, Teran FJ, Morales MDP, Veintemillas-Verdaguer S, Thanh NTK, Besenhard MO, Wilhelm C, Gazeau F, Harmer Q, Mayes E, Manshian BB, Soenen SJ, Gu Y, Millán Á et al (2021) Whither magnetic hyperthermia? A tentative roadmap. *Materials* 14(4):706
- Ruzicka-Ayoush M, Sobczak K, Grudzinski IP (2023) Comparative studies on the cytotoxic effects induced by iron oxide nanoparticles in cancerous and noncancerous human lung cells subjected to an alternating magnetic field. *Toxicol in Vitro* 95:105760. <https://doi.org/10.1016/j.tiv.2023.105760>
- Rylander MN, Feng Y, Zimmermann K, Diller KR (2010) Measurement and mathematical modeling of thermally induced injury and heat shock protein expression kinetics in normal and cancerous prostate cells. *Int J Hypertherm* 26(8):748–764. <https://doi.org/10.3109/02656736.2010.486778>
- Sapareto SA, Dewey WC (1984) Thermal dose determination in cancer therapy. *Int J Radiat Oncol Biol Phys* 10(6):787–800. [https://doi.org/10.1016/0360-3016\(84\)90379-1](https://doi.org/10.1016/0360-3016(84)90379-1)
- Scutigliani EM, Liang Y, Crezee H, Kanaar R, Krawczyk PM (2021) Modulating the heat stress response to improve hyperthermia-based anticancer treatments. *Cancers (basel)*. <https://doi.org/10.3390/cancers13061243>
- Shirvalilou S, Khoei S, Esfahani AJ, Kamali M, Shirvalilou M, Sheervalilou R, Mirzaghavami P (2021) Magnetic Hyperthermia as an adjuvant cancer therapy in combination with radiotherapy versus radiotherapy alone for recurrent/progressive glioblastoma: a systematic review. *J Neurooncol* 152(3):419–428. <https://doi.org/10.1007/s11060-021-03729-3>
- Siegel RL, Miller KD, Wagle NS, Jemal A (2023) Cancer statistics, 2023. *CA Cancer J Clin* 73(1):17–48. <https://doi.org/10.3322/caac.21763>

- Singh M, Gu Q, Ma R, Zhu L (2020) Heating protocol design affected by nanoparticle redistribution and thermal damage model in magnetic nanoparticle hyperthermia for cancer treatment. *J Heat Transfer*. <https://doi.org/10.1115/1.4046967>
- Song CW (1984) Effect of local hyperthermia on blood flow and microenvironment: a review. *Cancer Res* 44(10 Suppl):4721s–4730s
- Tang D, Khaleque MA, Jones EL, Theriault JR, Li C, Wong WH, Stevenson MA, Calderwood SK (2005) Expression of heat shock proteins and heat shock protein messenger ribonucleic acid in human prostate carcinoma in vitro and in tumors in vivo. *Cell Stress Chaperones* 10(1):46–58. <https://doi.org/10.1379/csc-44r.1>
- Tran TTD, Vo TV, Tran PHL (2015) Design of iron oxide nanoparticles decorated oleic acid and bovine serum albumin for drug delivery. *Chem Eng Res Design* 94:112–118. <https://doi.org/10.1016/j.cherd.2014.12.016>
- van Rhooen GC (2016) Is CEM43 still a relevant thermal dose parameter for hyperthermia treatment monitoring? *Int J Hyperthermia* 32(1):50–62. <https://doi.org/10.3109/02656736.2015.1114153>
- van Rhooen GC, Samaras T, Yarmolenko PS, Dewhirst MW, Neufeld E, Kuster N (2013) CEM43A°C thermal dose thresholds: a potential guide for magnetic resonance radiofrequency exposure levels? *Eur Radiol* 23(8):2215–2227. <https://doi.org/10.1007/s00330-013-2825-y>
- van Rhooen GC, Franckena M, ten Hagen TLM (2020) A moderate thermal dose is sufficient for effective free and TSL based thermochemotherapy. *Adv Drug Deliv Rev* 163:145–156. <https://doi.org/10.1016/j.addr.2020.03.006>
- Vaupel PW, Kelleher DK (2012) Blood flow and associated pathophysiology of uterine cervix cancers: characterisation and relevance for localised hyperthermia. *Int J Hypertherm* 28(6):518–527. <https://doi.org/10.3109/02656736.2012.699134>
- Vicentini M, Vassallo M, Ferrero R, Androulakis I, Manzin A (2022) In silico evaluation of adverse eddy current effects in preclinical tests of magnetic hyperthermia. *Comput Methods Programs Biomed* 223:106975. <https://doi.org/10.1016/j.cmpb.2022.106975>
- Viglianti BL, Dewhirst MW, Abraham JP, Gorman JM, Sparrow EM (2014) Rationalization of thermal injury quantification methods: application to skin burns. *Burns* 40(5):896–902. <https://doi.org/10.1016/j.burns.2013.12.005>
- Vujaskovic Z, Kim DW, Jones E, Lan L, McCall L, Dewhirst MW, Craciunescu O, Stauffer P, Liotcheva V, Betof A, Blackwell K (2010) A phase I/II study of neoadjuvant liposomal doxorubicin, paclitaxel, and hyperthermia in locally advanced breast cancer. *Int J Hypertherm* 26(5):514–521. <https://doi.org/10.3109/02656731003639364>
- Wang G, Xu D, Chai Q, Tan X, Zhang Y, Gu N, Tang J (2014) Magnetic fluid hyperthermia inhibits the growth of breast carcinoma and downregulates vascular endothelial growth factor expression. *Oncol Lett* 7(5):1370–1374. <https://doi.org/10.3892/ol.2014.1893>
- Westermann A, Mella O, Van der Zee J, Jones EL, Van der Steen-Banasik E, Koper P, Uitterhoeve ALJ, De Wit R, Van der Velden J, Burger C, Schem BC, Van der Wilt C, Dahl O, Prosnitz LR, Van Tinteren H (2012) Long-term survival data of triple modality treatment of stage IIB-III-IVA cervical cancer with the combination of radiotherapy, chemotherapy and hyperthermia—an update. *Int J Hypertherm* 28(6):549–553. <https://doi.org/10.3109/02656736.2012.673047>
- Westra A, Dewey WC (1971) Variation in sensitivity to heat shock during the cell-cycle of chinese hamster cells in vitro. *Int J Radiat Biol Relat Stud Phys Chem Med* 19(5):467–477. <https://doi.org/10.1080/09553007114550601>
- Yarmolenko PS, Moon EJ, Landon C, Manzoor A, Hochman DW, Viglianti BL, Dewhirst MW (2011) Thresholds for thermal damage to normal tissues: an update. *Int J Hypertherm* 27(4):320–343. <https://doi.org/10.3109/02656736.2010.534527>
- Yung JP, Shetty A, Elliott A, Weinberg JS, McNichols RJ, Gowda A, Hazle JD, Stafford RJ (2010) Quantitative comparison of thermal dose models in normal canine brain. *Med Phys* 37(10):5313–5321. <https://doi.org/10.1118/1.3490085>
- Zito Marino F, Bianco R, Accardo M, Ronchi A, Cozzolino I, Morgillo F, Rossi G, Franco R (2019) Molecular heterogeneity in lung cancer: from mechanisms of origin to clinical implications. *Int J Med Sci* 16(7):981–989. <https://doi.org/10.7150/ijms.34739>

Publisher's Note

Springer Nature remains neutral with regard to jurisdictional claims in published maps and institutional affiliations.